JOURNAL OF SOLID STATE CHEMISTRY **138,** 226–231 (1998)
ARTICLE NO. SC987801

Study of Structural, Magnetic, and Electrical Properties of $La_{2/3}Ca_{1/3}Mn_{1-x}In_xO_3$ Perovskites

M. C. Sánchez,[1] J. Blasco, J. García, J. Stankiewicz, J. M. De Teresa, and M. R. Ibarra

Departamento de Física de la Materia Condensada e Instituto de Ciencia de Materiales de Aragón, Universidad de Zaragoza-Consejo Superior de Investigaciones Científicas, 50009-Zaragoza, Spain

Received September 24, 1997; in revised form February 17, 1998; accepted February 24, 1998

The effect of the substitution of Mn with In in the magnetoresistive $La_{2/3}Ca_{1/3}MnO_3$ compound has been studied by means of X-ray diffraction, a.c. magnetic susceptibility, d.c. magnetization, and d.c. resistance techniques. This substitution is possible for $x \leq 0.07$ under normal synthetic procedures. The Curie temperature decreases with increasing x in $La_{2/3}Ca_{1/3}Mn_{1-x}In_xO_3$. Samples with $x \geq 0.05$ do not show long-range ferromagnetic order but rather a cluster-glass behavior. Magnetic inhomogeneities, arising both from random substitution of Mn with In and from formation of oxygen vacancies, can lead to such behavior. Samples with $x \geq 0.05$ do not show metal–insulator transition.

INTRODUCTION

The physical properties of $La_{1-y}A_yMnO_3$ (A = Ca, Ba, Sr) have been widely studied in the past (1–4). The discovery of giant magnetoresistance effects has renewed the interest in such compounds (5–7). $LaMnO_3$ and $AMnO_3$ are insulators (8–10), but the partial replacement of La^{3+} by divalent cations (Ca, Sr, or Ba) gives rise to a ferromagnetic ordering and metallic behavior (11) at low temperatures, in a narrow range of concentrations ($0.2 \leq y < 0.5$). Coexistence of ferromagnetism and metallic conduction in these materials was explained in the past by the double-exchange (DE) interaction (12, 13). Recently, an additional Jahn–Teller distortion has been proposed to explain the large magnetoresistance effects (14). Large volume anomalies have been found at the insulator–metal (MI) transition in these compounds by several techniques suggesting a charge localization with strong electron-lattice coupling (15–17). This has also been confirmed by measurements of the isotopic effect in some of these compounds (18). Furthermore, magnetic correlations have been observed well above T_c, and magnetic polaron formation has been proposed to explain the intrinsic magnetoresistance in these compounds (19).

The influence of the rare-earth replacement on the properties of manganites has been extensively studied (20–22). However, the effect of a partial replacement of Mn by another element is much less studied (23, 24). A better knowledge of the charge localization process above T_c can be achieved by destabilizing the Mn sublattice. Recently, we have studied the substitution of Mn with Al in the archetypal giant magnetoresistive compound $La_{2/3}Ca_{1/3}MnO_3$ (7). At $T_c \approx 260$ K, this compound undergoes a paraferromagnetic transition accompanied by an MI transition. The highest magnetoresistive ratio is obtained around this temperature (25). Al was chosen because it has no magnetic moment and its atomic radius is smaller than that of Mn. For low substitution values, a decrease of the T_c with increasing Al content is observed (7, 26), but the magnetoresistive properties do not change very much. For samples with $x \geq 0.1$, oxygen vacancies are formed in the lattice. The combined action of these vacancies and the random distribution of the Al atoms makes these compounds magnetically inhomogeneous.

In this paper, we present a complementary study on the effect of Mn replacement by In, which has no magnetic moment and larger atomic radius than Mn. Because of this difference in the ionic size, a strong effect of the substitution on the main physical properties is expected. Moreover, $LaInO_3$ has a pervoskite structure (27) so the $La_{2/3}Ca_{1/3}Mn_{1-x}In_xO_3$ solid solutions are expected to exist in a wide range of concentrations.

EXPERIMENTAL SECTION

$La_{2/3}Ca_{1/3}Mn_{1-x}In_xO_3$ (x = 0, 0.01, 0.03, 0.05) samples were prepared by standard ceramic procedures. Stoichiometric amounts of La_2O_3, $CaCO_3$, In_2O_3, and $MnCO_3$, with nominal purities not less than 99.99%, were mixed and heated in air at 950°C for 12 h. After grinding, they were pressed into bars and sintered in air at 1250°C for 48 h and at 1400°C for 12 h with intermediate grindings. Samples with x = 0, 0.03, 0.05, 0.07, 0.1, 0.15, and 0.3 were prepared

[1] To whom correspondence should be addressed.

0022-4596/98 $25.00

by using a sol–gel method to optimize the mixture of starting material. Stoichiometric amounts of La_2O_3, $CaCO_3$, $In(OH)_3$, and $MnCO_3$ were dissolved in nitric acid. After this, citric acid and ethylene glycol were added in a ratio of 4 g citric acid to 2 ml ethylene glycol and 1 g metal nitrates. The solutions were heated until they gave a brown gel. These gels were heated to the combustion point. No burst out of the gels occurred under these conditions; the result was a fine black-brown powder. These powders were calcined overnight at 950°C and then pressed at 5 kbar and sintered at 1200°C for 48 h and at 1400°C for 12 h with intermediate grindings. Samples obtained by different methods ($x = 0$, 0.03, and 0.05) showed identical physical properties. Density measurements of the pellets were made using the Archimedes method. All samples had densities around 85% of the theoretical value.

Step-scanned powder diffraction patterns were collected at room temperature using a D-Max Rigaku system with a rotating anode. The diffractometer was operated at 100 mA and 40 kV with a Cu anode and a graphite monochromator was used to select the Cu$K\alpha_{1,2}$ radiation. Data were collected from 18° up to 140° with a step size of 0.02° and a counting rate of 8 sec/step. The structures were refined by the full-pattern method using the program FULLPROF (28). A pseudo-Voigt function was used as the peak shape function, and an overall temperature factor was considered. The oxygen content was analyzed using standard redox titration with $KMnO_4$ and Mohr's salt.

Magnetic measurements were carried out between 5 and 300 K using a commercial Quantum Design (SQUID) magnetometer, with an a.c. option. The resistance measurements were performed by the six-probe method. Electrical contacts were prepared with silver paste on the bar-shaped samples.

RESULTS AND DISCUSSION

X-ray powder diffraction shows clean single-phase patterns for samples with $x \leq 0.07$. The diffractograms can be indexed in the *Pbnm* spatial group, the most commonly found when perovskites are orthorhombically distorted, in agreement with related compounds (11, 29). Figure 1 shows the diffractogram obtained for the $x = 0.07$ sample as an example. However, samples with $x \geq 0.1$ showed minor impurity phases in addition to the perovskite structure, as can be seen in the pattern for the $x = 0.15$ sample shown in Fig. 2. The impurities can be reasonably identified as $LaInO_3$ and $Ca_3In_2O_6$. The small range of solid solution can be ascribed to the large In^{3+} ionic size which gives rise to a miscibility gap in spite of the similarities between $LaMnO_3$ and $LaInO_3$ crystal structures. Table 1 shows the relevant structural parameters obtained from the profile analysis of the X-ray patterns for the $x \leq 0.07$ samples. The interatomic distances and angles for MnO_6 octahedra from the refined atomic positions are listed in Table 2. The cell

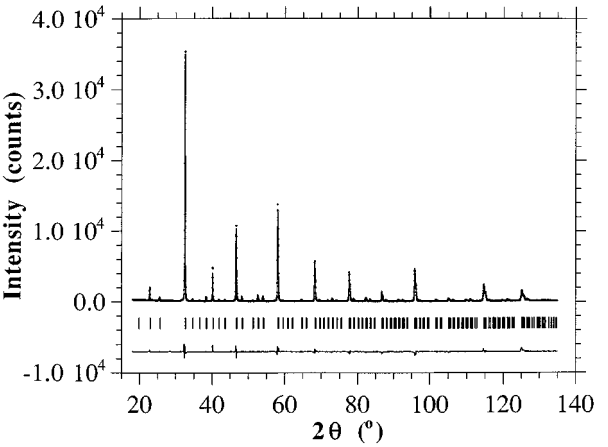

FIG. 1. X-ray powder pattern and best fit (continuous line) at room temperature for $La_{2/3}Ca_{1/3}Mn_{0.93}In_{0.07}O_3$. The difference is plotted at the bottom. The bars denote the calculated Bragg-reflected positions.

parameters and unit-cell volume increase with increasing In content, as expected as a result of the larger ionic size of In^{3+}. Consequently, the average Mn–O distance increases with increasing In content. Nevertheless, a different behavior is shown by the angles between neighboring octahedra. Even though the angle along the apical oxygen (i.e., Mn–O1–Mn) remains practically unchanged for all samples, the angle along the equatorial oxygen (i.e., Mn–O2–Mn) decreases with increasing In content. Therefore, the average Mn–O–Mn angle is also reduced for all compositions studied. The angles O–Mn–O are very close to 90° in the whole series, indicating a regular MnO_6 octahedron with the three Mn–O distances very similar and no static Jahn–Teller distortion.

Samples with low In content ($x \leq 0.03$) are nominally stoichiometric as measured by redox titration (Table 2).

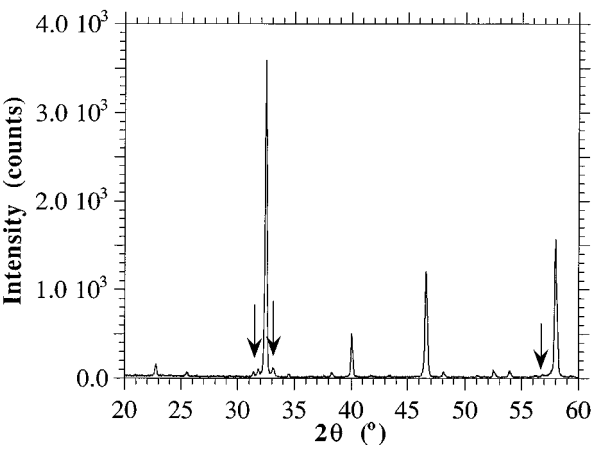

FIG. 2. X-ray diffractogram of $La_{2/3}Ca_{1/3}Mn_{0.85}In_{0.15}O_3$ at room temperature. Arrows indicate the main diffraction peaks of impurity phases detected.

TABLE 1

Refined Fractional Atomic Positions, and Average Debye–Waller, Unit-Cell and Reliability Factors (%) for $La_{2/3}Ca_{1/3}Mn_{1-x}In_xO_3$ at Room Temperature

	$x = 0$	$x = 0.01$	$x = 0.03$	$x = 0.05$	$x = 0.07$
La					
x	0.9965(2)	0.9955(8)	0.9969(1)	0.9972(6)	0.9965(7)
y	0.0187(1)	0.0193(4)	0.0198(2)	0.0213(7)	0.0221(6)
O(1)					
x	0.0588(14)	0.0638(3)	0.0593(6)	0.0611(1)	0.0595(8)
y	0.4916(8)	0.4886(8)	0.4932(6)	0.4937(5)	0.4907(6)
O(2)					
x	0.7219(11)	0.7209(4)	0.7206(8)	0.7198(8)	0.7192(1)
y	0.2786(11)	0.2818(6)	0.2807(4)	0.2799(1)	0.2814(1)
z	0.0333(6)	0.0314(5)	0.0342(8)	0.0365(7)	0.0396(3)
B (Å^2)	0.0[a]	0.32(4)	0.64(8)	0.92(9)	0.42(1)
a (Å)	5.4717(1)	5.4730(1)	5.4759(1)	5.4855(2)	5.4905(1)
b (Å)	5.4569(1)	5.4602(1)	5.4641(1)	4.4764(3)	5.4851(8)
c (Å)	7.7112(1)	7.7134(9)	7.7224(1)	7.7408(8)	7.7521(1)
V (Å^3)	230.24	230.50	231.06	232.54	233.46
R_p	9.5	7.9	7.4	7.4	8.1
R_{wp}	10.8	10.3	10.0	9.8	11.0
R_{exp}	5.9	5.3	4.9	4.5	5.3
χ^2	3.3	3.7	4.1	4.7	4.4
R_{bragg}	5.8	6.3	7.1	6.9	6.7

[a] In this sample, the overall temperature factor (B) has not been refined.

TABLE 2

Percentage of Mn^{4+} Content and Selected Interatomic Distances (Å) and Angles (deg) for the MnO_6 Octahedron of $La_{2/3}Ca_{1/3}Mn_{1-x}In_xO_3$ at Room Temperature

		$x = 0$	$x = 0.01$	$x = 0.03$	$x = 0.05$	$x = 0.07$
Mn^{4+} (%)		30	31	32	28	24
Mn–O(1)	2	1.955(1)	1.960(7)	1.958(2)	1.964(3)	1.966(1)
Mn–O(2)	2	1.959(6)	1.952(1)	1.960(9)	1.971(1)	1.977(1)
	2	1.963(6)	1.972(2)	1.970(6)	1.973(3)	1.981(2)
⟨Mn–O⟩		1.95(9)	1.96(1)	1.96(3)	1.96(9)	1.97(4)
Mn–Mn	2	3.855(1)	3.856(8)	3.861(2)	3.870(5)	3.876(1)
	4	3.864(1)	3.865(5)	3.867(9)	3.875(6)	3.880(5)
O(1)–Mn–O(2)	2	89.1(4)	89.2(5)	89.0(7)	88.6(4)	87.7(7)
	2	89.5(4)	89.8(9)	89.1(4)	88.9(1)	88.1(9)
	2	90.5(4)	90.1(1)	90.8(6)	91.0(9)	91.8(1)
	2	90.9(3)	90.7(4)	90.9(2)	91.3(6)	92.2(2)
O(2)–Mn–O(2)	2	88.9(4)	88.9(2)	88.8(1)	88.7(3)	88.5(5)
	2	91.1(4)	91.0(7)	91.1(9)	91.2(6)	91.4(5)
Mn–O(1)–Mn	2	160.9(3)	159.1(62)	160.7(55)	160.2(50)	160.6(10)
Mn–O(2)–Mn	4	160.4(14)	160.1(59)	159.3(59)	158.5(79)	157.2(41)
⟨Mn–O–Mn⟩		160.6	159.8	159.7	159.1	158.3

Nevertheless, the Mn^{4+} percentage decreases for higher In content, and oxygen vacancies are present for $x \geq 0.05$. For instance, the actual formula measured by redox titration for $x = 0.07$ is $La_{2/3}Ca_{1/3}Mn_{0.93}In_{0.07}O_{2.94\pm0.02}$. There are two mechanisms to preserve the charge equilibrium when Mn is replaced by In: formation of oxygen vacancies and oxidation from Mn^{3+} to Mn^{4+}. At low In concentrations ($x \leq 0.03$), the preponderant mechanism is the Mn^{3+} oxidation because the samples do not show oxygen vacancies. Nevertheless, for higher In concentrations, oxygen vacancies are formed. Similar effects have been detected in samples doped with A1 (7), in spite of the differences in the ionic size between Al^{3+} and In^{3+}.

Oxygen occupancies have not been refined by the full-pattern Rietveld method. A refinement of these parameters for 0.07 sample yields values of 1.05(3) and 1.90(4) for O(1) and O(2), respectively. Although these values are nearly equal to the stoichiometric values within standard errors, they seem to indicate that the oxygen vacancies are mainly located at the equatorial positions. In addition, the correlation observed between the concentration of oxygen vacancies and Mn–O2–Mn bond angle decrease seems to support this conclusion. A similar effect is found for $La_{2/3}Ca_{1/3}MnO_3$ samples doped with Al. In these samples, the oxygen vacancies are located at the O(1) position and a slight decrease in Mn–O1–Mn angle is observed. Therefore, there seems to exist a relationship between ionic size of the substituting atom and position of the oxygen vacancies.

Figure 3 shows a.c. magnetic susceptibility measurements of the series as a function of temperature. Overall, the replacement of Mn by In leads to weaker ferromagnetic interactions, and two different behaviors can be observed depending on the In content. The susceptibility curves of samples with $x \leq 0.03$ show a sharp jump corresponding to the ferromagnetic–paramagnetic phase transition. The T_c, defined as the inflexion point of the susceptibility curves, decreases strongly with the increase of the In content. This transition is very sharp for the undoped compound and is broader for the doped samples because of the higher degree of structural disorder in the Mn lattice.

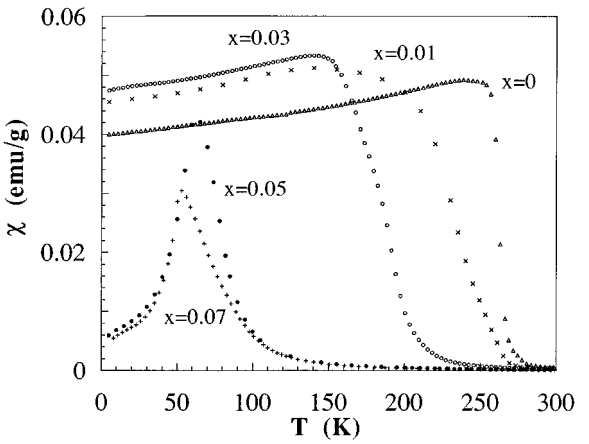

FIG. 3. The temperature dependence of the a.c. magnetic susceptibility for $La_{2/3}Ca_{1/3}Mn_{1-x}In_xO_3$ samples with $0 \leq x \leq 0.07$.

For $x \geq 0.05$, the jump corresponding to the ferromagnetic–paramagnetic phase transition disappears, and a peak appears at lower temperatures. Similar features were observed in $La_{2/3}Ca_{1/3}MnO_3$ doped with Al but for higher degree of substitution. These results indicate that the substitution of Mn by In leads to a much stronger decrease in the strength of the ferromagnetic interactions in $La_{2/3}Ca_{1/3}Mn_{1-x}In_xO_3$ compounds in comparison with other related compounds.

The $La_{2/3}Ca_{1/3}Mn_{1-x}In_xO_3$ samples do not follow the Curie–Weiss law in the range of temperatures studied (below 300 K). If the Curie–Weiss fit is forced in the range of temperatures between 200 and 300 K for $x = 0.05$ and 0.07 samples, the values obtained for the calculated paramagnetic effective magnetic moment (μ_{eff}) are 7.5 and 6 μ_B, respectively, far above the theoretical value ($\mu_t \approx 4.6\ \mu_B$), calculated as

$$\mu_t = \sqrt{x\mu^2_{Mn^{4+}} + (1-x)\mu^2_{Mn^{3+}}},$$

where 3.8 μ_B and 4.9 μ_B are the effective magnetic moments for Mn^{4+} and Mn^{3+}, respectively (30). This behavior indicates the presence of ferromagnetic interactions well above the magnetic transition.

Isothermal magnetization measurements up to 5 T at 5 K are shown in Fig. 4. Samples with $x \leq 0.03$ show a typical ferromagnetic behavior with a saturation magnetization value of about 92 emu/g, which corresponds to an effective magnetic moment of 3.45 μ_B. This value is similar to the saturation magnetization calculated in Refs. 1 and 3 for Mn^{3+}/Mn^{4+} ratios corresponding to our samples. For samples with $x = 0.05$ and 0.07, the M vs. H curves do not show saturation, indicating the absence of ferromagnetic order at low temperatures. Extrapolating the high field magnetization data for these samples to $H = 0$ T, we obtain a magnetic saturation of about 30 emu/g that corresponds to 1.1 μ_B per unit formula.

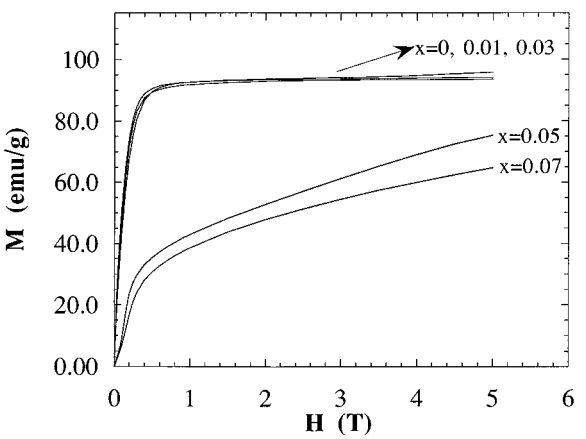

FIG. 4. Magnetization up to 5 T at 5 K for $La_{2/3}Ca_{1/3}Mn_{1-x}In_xO_3$ samples with $0.01 \leq x \leq 0.07$.

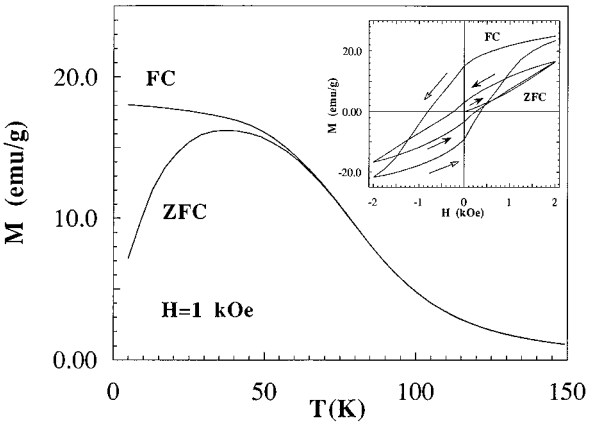

FIG. 5. FC and ZFC magnetization under a field of 1 kOe for the $La_{2/3}Ca_{1/3}Mn_{0.93}In_{0.07}O_3$ sample. The inset shows the ZFC and FC hysteresis at 5 K for this sample.

In order to understand the magnetic properties of $x \geq 0.05$ samples, low field magnetization measurements as a function of temperature were performed. Figure 5 shows the results obtained for the $x = 0.07$ sample. Magnetization was measured warming the samples under a field of 1 kOe, after they were cooled down from room temperature, first without applied field (zero field cooled, ZFC) and subsequently under applied field (field cooled, FC). The FC and ZFC magnetization curves start to separate at around 60 K, where a weak irreversibility begins to develop as a result of the freezing of the magnetic clusters. This is a feature of spin glass-like behavior, in agreement with the absence of long range ferromagnetism. The inset of Fig. 5 shows hysteresis loops obtained for the $x = 0.07$ sample between -2 kOe and 2 kOe under both FC and ZFC conditions. A symmetric loop is obtained under ZFC conditions, whereas for FC conditions a thermal remanent magnetization (TMR) is observed that changes with the field (H) giving rise to an asymmetric cycle. The FC induces a preferred direction with a small net ferromagnetic moment and causes the TRM. These features are hallmarks of a cluster-glass behavior (31).

As is well known, $La_{2/3}Ca_{1/3}MnO_3$ shows a MI transition at the para-ferromagnetic transition temperature, T_c. The resistivity as a function of temperature is displayed for the whole series in Fig. 6. Samples with low In content ($x \leq 0.03$) show a peak in their resistivity curves. As the In content increases, the value of resistivity at maximum increases, and the peak moves to lower temperatures. Doped samples with $x \leq 0.03$ show a broad maximum that can be attributed to the magnetic transitions shown in Fig. 3. Samples with a higher content of In show a semiconducting-type resistivity in agreement with the lack of a para-ferromagnetic transition in these samples.

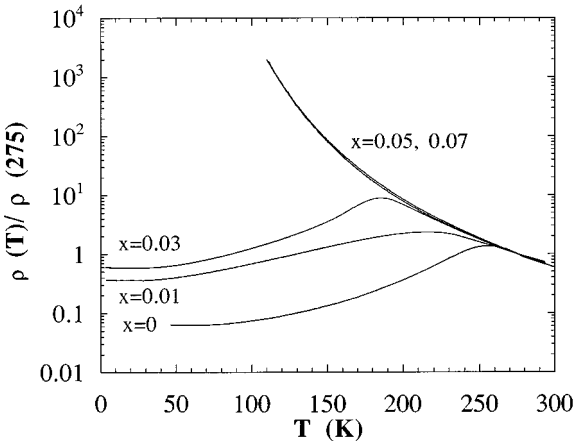

FIG. 6. Normalized resistivity vs. temperature curves for $La_{2/3}Ca_{1/3}Mn_{1-x}In_xO_3$ samples with $0 \leq x \leq 0.07$. The data have been normalized to the resistivity at 275 K.

The resistivity can be fitted to an Arrhenius law at temperatures above T_c for $x \leq 0.03$ samples and in the whole temperature range for $x = 0.05$ and 0.07 samples. The values of activation energies (E_a) obtained for all samples are practically equal, as can be inferred from the slope of the curves in Fig. 6, and range between 0.11 and 0.14 eV, showing a slight increase with increasing In content in the sample. Similar values of E_a have been reported in related samples (23).

In summary, the substitution of Mn with In leads to a decrease in T_c and MI transition; for $x > 0.03$ the $La_{2/3}Ca_{1/3}Mn_{1-x}In_xO_3$ samples are semiconducting with no long-range ferromagnetic ordering. The decrease of T_c can be related to a weakness of the DE ferromagnetic interaction in this series. It is well known that the DE interaction depends on both, the Mn–O distance and Mn–O–Mn bond angle (13). The introduction of In increases the average Mn–O distance and decreases the Mn–O–Mn bond angle as shown in Table 2. In addition, the oxygen vacancies are formed. These effects can qualitatively explain the decrease of T_c because they suppress the DE interaction. However, the changes in distances and angles are so small that they cannot account for the experimental features quantitatively, in particular for the suppression of MI transition and ferromagnetism at a low doping ratio ($x \geq 0.05$). Moreover, these compounds show local ferromagnetic correlations above T_c as seen from magnetic measurements. Similar correlations has been detected in related compounds by neutron diffraction techniques (32) well above T_c. They have been explained on the basis of magnetic polaron formation above T_c (19). The magnetic polaron size grows with decreasing temperature, giving rise to long-range ferromagnetism at T_c. Our experimental results in samples doped with In seem to indicate that ferromagnetic clusters are formed at high temperatures but that they are unable to develop long-range ferromagnetism at low temperatures. Similar features have been observed in related series such as $La_{2/3}Ca_{1/3}Mn_{1-x}Al_xO_3$ (7) and $La_{2/3}Ca_{1/3}Mn_{1-x}Co_xO_3$ (33). They have been explained on the basis of local disorder due to both substitution of Mn with a foreign element and oxygen vacancies. The disorder in Mn and O sublattices can lead to a localization of ferromagnetic clusters, thus excluding the formation of ferromagnetism. Furthermore, it produces magnetic frustration in the Mn sublattice giving rise to samples with a cluster-glass behavior.

Nevertheless, we want to emphasize that the changes produced by the substitution of Mn with In are larger than these produced by the substitution with Al or Co. This implies an intrinsic effect in the substitution with In that we ascribe to the larger ionic size of In^{3+}. Our results show that an almost perfect Mn lattice is necessary to produce ferromagnetic and metallic state.

CONCLUSIONS

$La_{2/3}Ca_{1/3}Mn_{1-x}In_xO_3$ samples can be obtained up to a value of $x = 0.07$ by means of conventional synthetic procedures. The substitution of Mn with In strongly changes the properties of the undoped compound. The T_c decreases along the series and the long-range ferromagnetism disappears in $x \geq 0.05$ samples, for which a cluster-glass behavior is observed. This can be explained by a magnetic disorder favored by both the decrease in the number of pathways between adjacent Mn atoms by the addition of In and the formation of oxygen vacancies. Local ferromagnetic interactions are observed at high temperatures in this series, but they are unable to develop long-range ferromagnetism at low temperatures because of the disorder in the lattice that occurs in related systems. Furthermore, this effect is enhanced by the large ionic size of In^{3+}.

The electrical behavior of this series reflects their magnetic properties. For small In content, there is a metal–insulator transition at T_c, whereas, the samples with $x \geq 0.05$ show a semiconducting behavior in the whole temperature range studied.

ACKNOWLEDGMENTS

The authors acknowledge the financial support of DGICYT under Projects Nos. MAT 96-0491 and MAT96-826.

REFERENCES

1. G. H. Jonker and J. H. van Santen, *Physica* **16,** 337 (1950).
2. J. B. Goodenough, *Phys. Rev.* **100,** 564 (1995).
3. G. H. Johner, *Physica* **22,** 707 (1956).
4. J. B. Goodenough, A. Wold, R. J. Arnott, and N. Menyuk, *Phys. Rev.* **124,** 373 (1961).

5. P. Mahendiran, A. K. Raychaudhuri, A. Chainani, D. D. Sarma, and S. B. Roy, *Appl. Phys. Lett*. **66,** 233 (1995).
6. M. McCormack, S. Jin, T. H. Tiefel, R. M. Fleming, J. M. Phillips, and R. Ramesh, *Appl. Phys. Lett*. **64,** 3045 (1994). S. Jin, H. M. O'Bryan, T. H. Tiefel, M. McCormack, and W. W. Rhodes, *Appl. Phys. Lett*. **66,** 382 (1995).
7. J. Blasco, J. Garcia, J. M. De Teresa, M. R. Ibarra, J. Perez, P. A. Algarabel, and C. Marquina, *Phys. Rev. B* **55,** 8905 (1997).
8. J. B. Goodenough and J. M. Longo, "Crystallographic and Magnetic Properties of Perovskite and Perovskite-related Compounds," Group III, vol. 4(a). Landolt-Börnstein, Berlin, 1970.
9. G. Matsumoto, *J. Phys. Soc. Jpn.* **29,** 606 (1970).
10. E. O. Wollan and W. C. Koehler, *Phys. Rev.* **100,** 545 (1955).
11. Y. Marimoto, A. Asamitsu, and Y. Yokura, *Phys. Rev. B* **51,** 16491 (1995).
12. C. Zener, *Phys. Rev. B* **82,** 403 (1951).
13. P. G. de Gennes, *Phys. Rev*. **118,** 141 (1960).
14. A. J. Millis, P. B. Zitlewood, and B. I. Shraiman, *Phys. Rev. Lett*. **74,** 5144 (1995).
15. M. R. Ibarra, P. A. Algarabel, C. Marquina, J. Blasco, and J. Garcia, *Phys. Rev. Lett*. **75,** 3541 (1995).
16. H. Roder, J. Zhang, and A. Bishop, *Phys. Rev. Lett*. **76,** 1356 (1996).
17. K. H. Kim, J. Y. Gu, H. S. Choi, G. W. Park, and T. W. Noh, *Phys. Rev. Lett*. **77,** 1877 (1996).
18. G.-M. Zhao, K. Conder, M. Keller, and K. A. Müller, *Nature* **381,** 676 (1996).
19. J. M. De Teresa, M. R. Ibarra, P. A. Algarabel, C. Ritter, C. Marquina, J. Blasco, J. Garcia, A. del Moral, and Z. Arnold, *Nature* **386,** 256 (1997).
20. H. Y. Hwang, S. W. Cheong, P. G. Radaelli, M. Marezio, and B. Batlogg, *Phys. Rev. Lett*. **75,** 914 (1995).
21. V. Caignaert, A. Maignan, and B. Raveau, *Solid State Commun.* **95,** 357 (1995).
22. J. Blasco, J. Garcia, J. M. De Teresa, M. R. Ibarra, P. A. Algarabel, and C. Marquina, *J. Phys. Condens. Matter* **8,** 7427 (1996).
23. R. Gundakaram, A. Arulraj, P. V. Vanitha, C. N. R. Rao, N. Gayathri, A. K. Raychaudhuri, and A. K. Cheetham, *J. Solid State Chem.* **127,** 354 (1996).
24. C. Martin, A. Maignan, and B. Raveau, *J. Mater. Chem.* **6,** 1245 (1996).
25. P. Schiffer, A. P. Ramirez, W. Bao, and S.-W. Cheong, *Phys. Rev. Lett*. **75,** 3336 (1995).
26. G. Turilli and F. Licci, *Phys. Rev. B* **54,** 13052 (1996).
27. S. Geller, *Acta Crystallogr*. **1,** 1948 (1967).
28. J. L. Rodriguez-Carvajal, *Physica B* **192,** 55 (1992).
29. J. M. De Teresa, J. Blasco, M. R. Ibarra, J. Garcia, C. Marquina, P. A. Algarabel, and A. del Moral, *Solid State Commun.* **96,** 627 (1995).
30. A. K. Cheetham and P. Day, "Solid State Chemistry: Techniques," p. 135. Oxford University Press, Oxford, 1987.
31. J. A. Mydosh, "Spin Glasses: An Experimental Introduction," p. 45. Taylor & Francis, London, 1993.
32. J. M. De Teresa, M. R. Ibarra, J. Blasco, J. Garcia, C. Marquina, P. A. Algarabel, Z. Arnold, K. Kamenev, C. Ritter, and R. von Helmolt, *Phys. Rev. B* **54,** 1187 (1996).
33. N. Gayathri, A. K. Raychaudhuri, S. K. Tiwary, R. Gundakaram, A. Arulraj, and C. N. R. Rao, *Phys. Rev. B* **56,** 1345 (1997).